JOURNAL OF THE AMERICAN CHEMICAL SOCIETY

Article

pubs.acs.org/JACS

Highly Selective, Facile NO_2 Reduction to NO at Cryogenic Temperatures on Hydrogen Precovered Gold

Ming Pan,[†] Hyung Chul Ham,[†,§] Wen-Yueh Yu,[†] Gyeong S. Hwang,[†] and C. Buddie Mullins*[,†,‡]

[†]Department of Chemical Engineering and [‡]Department of Chemistry and Biochemistry, Center for Nano and Molecular Science and Technology, Texas Materials Institute, and Center for Electrochemistry, University of Texas at Austin, Austin, Texas 78712-0231, United States

Supporting Information

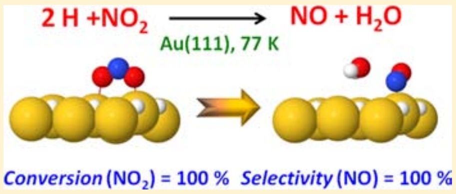

ABSTRACT: We have discovered that NO_2 is reduced to NO at 77 K by hydrogen precovered gold in vacuum. Here, we investigate the partial reduction of NO_2 to NO on an atomic-hydrogen populated model gold catalyst for a more fundamental understanding of the surface chemistry of hydrogenation. Gold-based catalysts have been found to be active for many hydrogenation reactions, but few related fundamental studies have been conducted. Our experimental results reveal a high catalytic activity for gold: indeed, NO_2 is reduced to NO with 100% conversion and 100% selectivity at temperatures lower than 120 K. Density functional theory calculations and reflection−absorption infrared spectroscopy measurements indicate that HNO_2 and N_2O_3 are intermediates which are highly dependent on surface hydrogen concentrations; subsequent hydrogenation of HNO_2 and dissociation of N_2O_3 upon annealing induces the production of NO and H_2O.

1. INTRODUCTION

Gold-based catalysts have been studied for a wide range of energy-efficient processes[1−12] as well as for hydrogenation chemistry.[13−21] NO_x reduction is also a potential application for gold catalysts and has been briefly investigated with H_2,[22,23] propene,[24] or CO[25,26] as reducing agents, but the mechanisms are not well understood. Here, we report a mechanistic study of NO_2 reduction to NO by atomic hydrogen using a model gold catalyst. The experimental results indicate that NO_2 can be converted to NO on H/Au(111) at a cryogenic temperature, 77 K. Unexpectedly high NO_2 conversion (100%) and NO selectivity (100%) are observed at temperatures lower than 120 K suggesting a highly selective and facile NO_2 reduction process mediated by the gold surface. Our previous work shows that atomic H has a small desorption activation energy of ~0.29 eV on Au(111),[27,28] so these weakly chemisorbed hydrogen adatoms likely play a key role in facilitating such unique hydrogenation chemistry. Density functional theory (DFT) calculations and reflection−absorption infrared spectroscopy (RAIRS) measurements provide insights into the relevant reaction mechanisms in which surface-bound HNO_2 and N_2O_3 are intermediates.

In this work, we employ a Au(111) single crystal as the model catalyst which can be considered as a planar representative of supported gold nanoparticles. In addition, since molecular hydrogen has a high energetic barrier to dissociation on model gold surfaces,[29,30] we employ gas-phase H atoms to populate the surface so that hydrogenation chemistry can be studied. We hope that our study will assist in identifying the role of gold on classical supported catalysts where H_2 dissociates on the periphery sites and likely spills over onto the gold particles.[31] Although this work only yields NO_2 reduction to NO, high conversion of NO_2 and high selectivity to NO have been observed, indicating unique surface chemistry for gold and providing insights into its catalytic activity in hydrogenation reactions.

2. EXPERIMENTAL SECTION

2.1. Experimental Apparatus and Sample Cleaning. All experiments were conducted in a supersonic molecular beam apparatus under ultrahigh-vacuum (UHV) conditions with a base pressure of 2×10^{-10} Torr.[32−35] The differentially pumped chamber consists of a source chamber to generate molecular beams and a scattering chamber for analysis, which contains a quadrupole mass spectrometer (QMS), an Auger electron spectrometer (AES), and low-energy electron diffraction (LEED) optics. A circular gold sample is installed on a pair of copper power leads which can be cooled to 77 K by a liquid nitrogen reservoir and resistively heated to 900 K by a proportional−integral−derivative (PID) controller. A K-type thermocouple was applied to measure sample temperatures. Prior to every experiment, the sample was cleaned by exposing to an intense NO_2 molecular beam with the surface held at 800 K for 2 min.[36,37] Periodically, contamination on the sample was removed by Ar^+ ion bombardment. The sample cleanliness and surface structure were verified by AES and LEED. Infrared (IR) measurements were carried out in another UHV chamber which has a Fourier transform infrared spectrometer and a mercury−cadmium−telluride (MCT) detector.[38]

2.2. Reactant Dosing. We employed a home-built device to generate H atoms via an electron-beam-heated high-temperature tungsten capillary in which molecular hydrogen is converted to H atoms or vibrationally excited molecules which dissociate on Au(111) at 77 K.[39,40] The relative coverage of hydrogen and deuterium atoms is determined by comparing to the saturated surface. In order to avoid NO_2 decomposition and purity degradation, the gas handling system,

Received: October 3, 2012
Published: December 11, 2012

dx.doi.org/10.1021/ja3096575 | *J. Am. Chem. Soc.* 2013, 135, 436−442

including valves and tubes, was passivated by exposing to a relatively high pressure of NO_2 for a prolonged time. NO_2 was delivered onto the Au(111) surface via a molecular beam initiating from a device with an array of nozzles, each with the same aperture size and separate plumbing to ensure reagent purity as delivered to the sample. The coverage of NO_2 is determined based on temperature programmed desorption (TPD) spectra from Au(111), where 1 monolayer (ML) nitrogen dioxide is considered as the amount yielding a maximum integrated area under the monolayer desorption feature. Water was introduced onto the sample surface in a molecular beam with a flux rate of 0.067 ML/sec.[35,41]

2.3. DFT Calculations. The calculations reported herein were performed on the basis of spin polarized DFT within the generalized gradient approximation (GGA-PW91),[42] as implemented in the Vienna ab-initio simulation package (VASP).[43] The projector augmented wave (PAW) method with a planewave basis set was employed to describe the interaction between core and valence electrons.[44] An energy cutoff of 350 eV was applied for the planewave expansion of the electronic eigenfunctions. For the Brillouin zone integration, we used a $(4 \times 4 \times 1)$ Monkhorst–Pack mesh of k points to calculate geometries and total energies. Reaction pathways and barriers were determined using the nudged elastic band method (NEBM) with eight intermediate images for each elementary step.[45] For Au model surfaces, we constructed a four atomic-layer slab with a hexagonal 3×3 unit cell. The slab is separated from its periodic images in the vertical direction by a vacuum space corresponding to seven atomic layers. The lattice constant for bulk Au is predicted to be 4.18 Å, close to the experimental value of 4.08 Å. While the bottom two layers of the four-layer slab were fixed at corresponding bulk positions, the upper two layers were fully relaxed using the conjugate gradient method until residual forces on all the constituent atoms became smaller than 5×10^{-2} eV/Å.

3. RESULTS AND DISCUSSION

3.1. NO Evolution From H/Au(111) via NO_2 Reduction at 77 K. We first performed molecular beam reactive scattering (MBRS) experiments to investigate the reduction of NO_2 on gold. A molecular beam-blocking shutter can be rapidly moved out/in of the path of the beam allowing/stopping the impingement of NO_2 molecules (the beam flux rate is 0.1 ML/sec with a kinetic energy of ~0.1 eV) on the Au(111) surface. A quadrupole mass spectrometer (QMS) was used to identify gas-phase species reacting/scattering from the sample. Figure 1 displays QMS signals from species evolving from the sample during the 20 s of NO_2 (2.0 ML) impingement onto both clean and H ($\theta_{H,rel} = 1$) preadsorbed Au(111) at a surface temperature of 77 K. Figure 1a illustrates a control experiment: Here NO_2 was impinged onto the clean Au(111) surface [without precovering the gold with H atoms] at $t = 0$ s where NO_2 molecules both adsorb and scatter off the sample and cause the QMS intensity increase observed. As the NO_2 beam strikes the surface over the entire 20 s experiment, a constant intensity for scattered NO_2 is observed, suggesting that scattering/adsorption of NO_2 dominates this process (with no hint of reaction).

With the Au(111) surface covered by H atoms at unity relative coverage (determined by comparing to a H-saturated sample surface), the MBRS experiments were performed with results shown in Figure 1b, indicating the evolution of NO from the surface at 77 K. Note that the sticking probability of NO_2 is ~60% on H-covered Au(111). In the initial ~4–5 s of impingement by the NO_2 beam, the NO signal shows virtually identical behavior to the experiment on clean Au(111) as shown in Figure 1a, suggesting an induction period. From $t = 5$ to 15 s, the signal for NO shows a significant evolution lasting for approximately 10 s and reaching a peak value at $t = 10$ s, demonstrating a reaction between adsorbed NO_2 and H adatoms. The points labeled from (i–v) indicate various experimental stages including (i) beam on, (ii) beginning, (iii) peak, (iv) end of NO evolution, and (v) beam off, respectively, which are discussed later with regard to relevant TPD measurements, DFT calculations, and RAIRS studies. In contrast to NO, the NO_2 signal behaves similarly as in the control experiment, with a constant intensity. We also observe that the MBRS experiment results in H_2 evolution at 77 K. This phenomenon is also likely related to NO_2 reduction, which activates H atoms and induces the desorption of H_2 at low temperature.

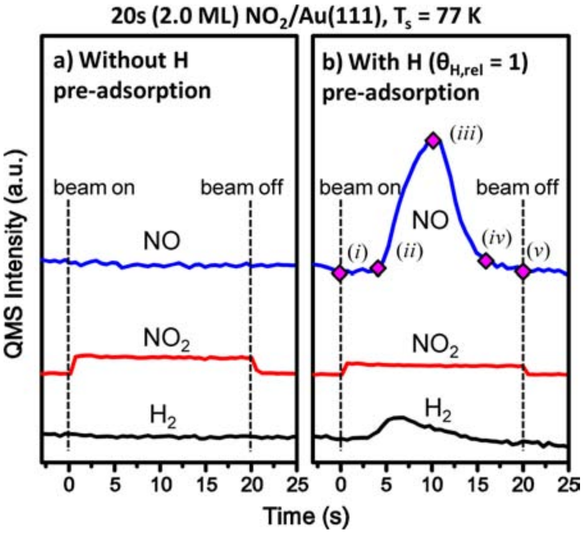

Figure 1. MBRS of NO_2. The beam strikes onto (a) the clean Au(111) surface (b) the H (relative coverage $\theta_{H,rel} = 1$) atom precovered Au(111) surface at 77 K. The NO_2 beam was impinged on the surface from 0 to 20 s. The points denoted (i–v) mark specific times corresponding to measurements discussed later in the paper. The NO_2 beam flux is 0.1 ML/sec. Note that (a,b) have the same Y-axis scale.

Note that both gaseous NO_2 and NO give signals for mass 30 in our mass spectrometer. For NO_2, the signal for mass 30 arises from the gas-phase dissociation (into NO and O) of the molecule in the electron bombardment ionization process, whereas for NO mass 30 is the parent mass. Thus, the MBRS spectra for NO in Figure 1 have been modified by subtracting the mass 30 component due to NO_2 from the signals at mass 30 in order to provide a better description of the NO evolution during NO_2 impingement on H/Au(111). The unaltered data are shown in Figure S1.

3.2. TPD Measurements Regarding the Different Reaction stages. To further explore the mechanistic details of this reaction, we conducted TPD measurements as a function of NO_2 coverage on the H-precovered ($\theta_{H,rel} = 1$) Au(111) surface at 77 K. The various NO_2 coverages are correlated to impingement times of the NO_2 beam and various stages of the reaction [i.e., points (i–v) displayed in Figure 1b]. Figure 2a,b displays TPD spectra for masses 30, 46, and 18, respectively, corresponding to NO + NO_2, NO_2, and H_2O, evolving from Au(111) upon heating the sample surface from 77 to 300 K at a ramp rate of 1 K/s. The black curves are acquired from a control experiment with unity relative H coverage on Au(111) but zero coverage of NO_2 (corresponding to point (i) in Figure 1b), in which, as expected, no desorption products for masses 30, 46, or 18 are observed.

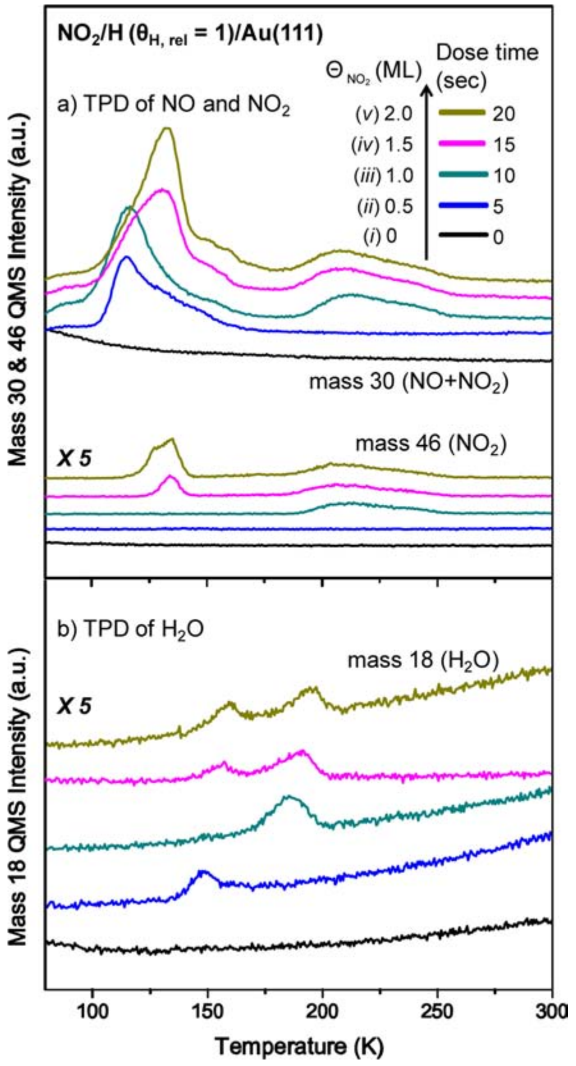

Figure 2. TPD studies from NO$_2$ and H coadsorbed Au(111). TPD spectra of mass 30, 46, and 18 after various coverages of NO$_2$ impingement to Au(111) with preadsorption of hydrogen atoms (relative coverage $θ_{H,rel}$ = 1) at 77 K. Note that (a) and (b) have the same scale for the *Y*-axis.

Next we studied the H/Au(111) surface ($θ_{H,rel}$ = 1) coadsorbed with 0.5 ML of NO$_2$ [this is equivalent to 5 s of NO$_2$ impingement and reaches the point at which the evolution of NO begins; i.e., point (ii) in Figure 1]. There is no desorption feature observed from the TPD spectrum for mass 46 indicating that the adsorbed NO$_2$ has completely reacted with the H adatoms yielding a 100% conversion. The TPD spectrum for mass 30 in Figure 2a shows a desorption feature with a peak at ~120 K, which can be completely attributed to desorbing NO rather than a mass fragment of NO$_2$ (since no mass 46 desorbs). During the measurement, no other reduced products, such as N$_2$O, N$_2$, or NH$_3$ were detected indicative of a high selectivity (100%) toward NO.

TPD measurements from the H-precovered ($θ_{H,rel}$ = 1) Au(111) surface after 10 s of NO$_2$ impingement were performed as shown in Figure 2a. This exposure of NO$_2$ results in a coverage of 1.0 ML and produces the maximum in NO evolution in MBRS [point (iii) in Figure 1b]. In the TPD measurements shown in Figure 2, the sample was heated to 300 K inducing a single broad feature from ~190–260 K in the spectrum for mass 46 indicative of NO$_2$ monolayer desorption, which is also apparent in mass 30 as the ionized fragment of NO$_2$. However, a significant desorption feature for mass 30 also appears with a peak at ~120 K. This feature is not duplicated in mass 46 and clearly suggests NO$_2$ reduction on the surface with subsequent NO desorption.

Point (iv) in Figure 1 indicates that the evolution of NO nearly vanishes after 15 s of NO$_2$ impingement (1.5 ML) on the H precovered Au(111) surface. On a comparably covered surface, the TPD experiment produces two desorption features with similar shape for both mass 30 and 46 (Figure 2a), in which peak temperatures are consistent with the distinct desorption features of NO$_2$ from clean Au(111).[46] Thus, we infer that the mass 30 signal is primarily (but not exclusively) from NO$_2$ fragmentation with little parent NO. Note that with decreasing H surface concentration [no detection of H$_2$ desorption at point (iv) indicating that H atoms are completely consumed] and a constant NO$_2$ beam flux, a portion of the NO$_2$ molecules directly adsorb on Au(111) without reacting and also contribute to the desorption features we measure in Figure 2a. We estimate that the evolved NO after point (iv), as shown in Figure 1b, is from ~6.1% of the total NO$_2$ molecules that have absorbed on the surface during 15 s of NO$_2$ beam impingement. Further extending the NO$_2$ impingement time until 20 s [point (v) in Figure 1b] results in a larger desorption feature for NO$_2$ in mass 30 and 46 at ~130 K as shown in Figure 2a, when the surface reactions are ending, and NO$_2$ is beginning to populate the multilayer on Au(111).

Figure 2b displays TPD spectra for water produced from the surface reaction between H adatoms and adsorbed NO$_2$ molecules on Au(111). The black curve illustrates a control experiment indicating, as expected, no water formation on the solely H-covered surface. With increasing NO$_2$ coverage on the H-precovered surface, water desorption sequentially yields for point (ii) a single peak at ~150 K [consistent with the characteristic desorption peak of water on clean Au(111)],[47] for (iii) a single peak at ~190 K and for (iv) and (v) two features apparent at both ~160 and ~190 K. This water desorption behavior is likely related to the progress of reaction involving H adatoms and NO$_2$ as well as their concentrations on the surface and will be discussed more later.

3.3. DFT Calculations to Explore Mechanisms for NO Evolution.

The results of our DFT calculations are summarized in Table 1 for which two types of surfaces have been compared regarding the H adatom coverage on Au(111) (here a low hydrogen coverage, $θ_H$, corresponds to more empty sites, represented by $θ_E$). Figure 3 shows a representative

Table 1. Energetics/Barriers of Surface Reactions During MBRS Experiments

	$θ_H$ ~ 1 ($θ_E$ ~ 0)		$θ_H$ ~ 0 ($θ_E$ ~ 1)	
reaction	Δ*E* (eV)	E_a (eV)	Δ*E* (eV)	E_a (eV)
(i–ii) Induction				
NO$_2$(g) → NO$_2$	−0.30		−0.81	
NO$_2$ + H → H$_{dw}$ONO	−1.13	0.04	−0.45	0.55
H$_{dw}$ONO → H$_{up}$ONO	−0.02	0.28	−0.24	0.35
(ii–iv) NO Evolution				
H + H$_{up}$ONO → NO + H$_2$O	−0.72	0.47	−0.90	0.30
NO + NO$_2$ → N$_2$O$_3$			−0.03	0.27
(iv– v) Postevolution				
NO$_2$(g) → NO$_2$			−0.81	

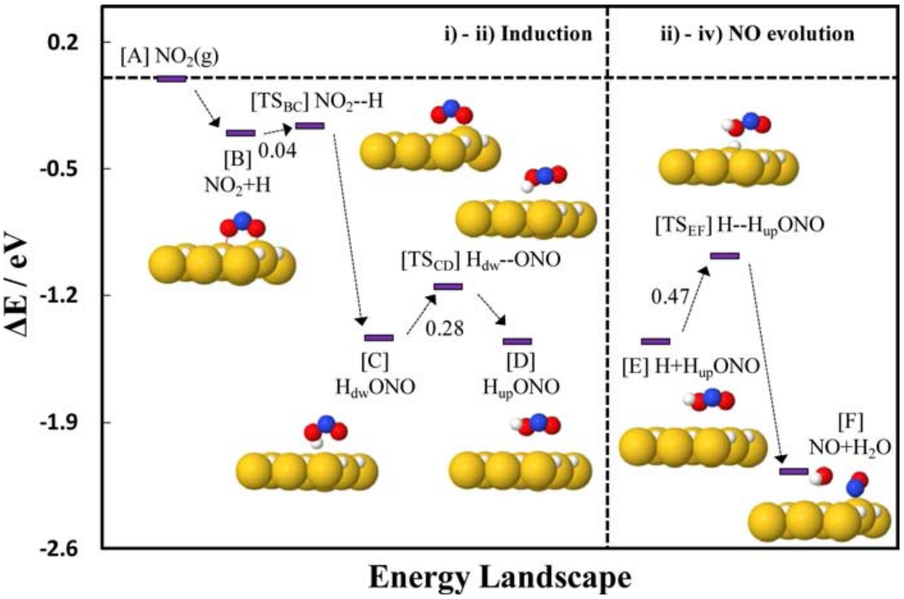

Figure 3. Predicted potential energy diagram for NO evolution from the NO_2 and H coadsorbed Au(111) surface. This diagram indicates the intermediate and transition-state configurations on Au(111) with high precovered H at $\theta_H = 1$. Note that the configurations of surface species are not affected by H coverages. The big yellow and the small blue, red, and white balls indicate Au, N, O, and H atoms, respectively.

energy diagram for NO_2 reduction and NO evolution on Au(111) at $\theta_H = 1$, illustrating species adsorption and transition states. It should be noted that the geometric configurations of molecules and intermediates on the surface are independent of surface H concentrations (i.e., the schematic configurations in Figure 3 are the same for low H coverage).

We first investigate the initial NO_2 activation on H covered Au(111) by calculating the adsorption energy of NO_2 and the reaction energetic/barrier for $NO_2 + H \rightarrow HNO_2$. As shown in Figure 3 and Table 1, we find that on the H saturated surface ($\theta_H \sim 1$ or $\theta_E \sim 0$), NO_2 exothermically adsorbs [$E_{ad} = 0.30$ eV] at the top-bridge-top site with the two O moieties of NO_2 bonded to Au atoms on H covered Au(111). In the next step, we see that adsorbed NO_2 can readily react with neighboring H adatoms with a very low barrier (0.04 eV), producing a *cis* form of HNO_2 (indicated by $H_{dw}ONO$ where H points toward the surface). Here, the rotational barrier of the H atom in $H_{dw}ONO$ for forming a *trans* HNO_2 ($H_{up}ONO$ where H points away from the surface) is predicted to be 0.28 eV. Together with the exothermic NO_2 adsorption energy, this result suggests that NO_2 can be trapped in the form of $H_{dw}ONO$ or $H_{up}ONO$ on H-covered Au(111) at 77 K.

This process dominates the early period in the MBRS measurement from 0–5 s and represents the initial induction period [the period (i–ii)] before the evolution of NO, as shown in Figure 1b. The computational results display the relatively high barriers for the reaction of HNO_2 with neighboring H atoms during the induction period ($H + H_{up}ONO \rightarrow NO + H_2O$, $E_a = 0.47$ eV. Note that we only focus on the $H_{up}ONO$ state because the reaction between $H_{dw}ONO$ and H always occurs via the $H_{up}ONO$ state), implying that NO cannot evolve at 77 K. Our TPD results show desorption peaks for NO and H_2O at ~120 and ~150 K, respectively, as displayed in Figure 2a,b. We also compared other possible reaction mechanisms for NO production, such as $NO_2 \rightarrow NO + O$ ($E_a = 1.98$ eV) and $H_{up}ONO \rightarrow NO + OH$ ($E_a = 0.81$ eV), both of which have a higher energetic barrier and cannot be considered viable mechanisms. Due to the high barrier for HONO dissociation and the ease of NO_2 trapping by H adatoms (which is exothermic by 1.13 eV), we think that the single-step Eley–Rideal (ER) reaction of $NO_2(g) + H \rightarrow OH + NO(g)$ is highly unlikely. In addition, the induction period we observe also indicates that the reduction of NO_2 to NO is not following an ER mechanism. Otherwise, NO would evolve immediately after the NO_2 beam strikes the H/Au(111) surface (at $t = 0$ s).

With further exposure of NO_2 to the surface by the beam, NO begins to evolve from the surface. This production of NO at 77 K is related to the reduction of the barrier for the reaction $H + H_{up}ONO \rightarrow NO + H_2O$ due to the increase of available empty surface sites near $H_{up}ONO$ (called "near empty sites" in later discussion) through H_2 desorption which has been observed during MBRS as shown in Figure 1b. Our previous study indicated that H atoms weakly chemisorb on Au(111) and H_2 recombinative desorption has a small activation energy of ~0.29 eV.[27,48] In contrast, the adsorption of NO_2 on H/Au(111) and HNO_2 formation is an exothermic process and releases heat (0.30 and 1.13 eV, respectively as shown in Table 1), which likely activates a fraction of the H adatoms leading to recombinative H_2 desorption at 77 K.

According to our DFT calculations, the barrier for $H + H_{up}ONO \rightarrow NO + H_2O$ strongly depends on the number of near empty surface sites around HNO_2. A larger number of near empty surface sites leads to a lower reaction barrier. In Table 1, we display the barriers for the surface reaction $H + H_{up}ONO \rightarrow NO + H_2O$ for different coverages of neighboring empty surface sites around HNO_2. We find that the barrier ($E_a = 0.30$ eV) at $\theta_E \sim 1$ is substantially lower than the $\theta_E \sim 0$ case ($E_a = 0.47$ eV), implying that the large availability of near empty surface sites around HNO_2 plays an important role in enhancing NO evolution through the $H + H_{up}ONO$ reaction at 77 K. Therefore, it can be concluded that the induction period prior to NO evolution at 77 K is partly due to the time needed for generation of near empty sites. Figure S2a shows that lower initial H coverages cause a longer induction period and smaller production of NO during MBRS, indicating that the formation of HNO_2 is a rate-determining step which is promoted by high coverage of H adatoms as shown in Table 1. These results suggest that NO evolution is not only affected by reaction kinetics but also influenced thermodynamically. The use of deuterium lengthens the induction period and significantly reduces the production of NO by a factor of 10, as shown in Figure S2b. These experimental results could be due to quantum tunneling of H/D and a primary kinetic isotope effect.

Additionally, a portion of the nascent NO directly evolves from the surface at 77 K, whereas the other part reacts with adsorbed NO_2 on the Au(111) surface via the reaction $NO + NO_2 \rightarrow N_2O_3$ where dinitrogen trioxide is generated as the second intermediate (DFT calculations show a barrier of 0.27 eV for $NO + NO_2 \rightarrow N_2O_3$). Annealing the sample surface causes the thermal dissociation of intermediate N_2O_3 producing NO and NO_2 as shown in Figure 2a(iii). TPD measurements indicate that H adatoms are depleted at the end of NO evolution ($t = \sim 15$ s). During the period from point (iii) to (v) in Figure 1b, a large fraction of NO_2 molecules adsorb intact on the surface with low reaction probability due to the lack of H adatom coverage.

DFT calculations indicate that water is produced from the reactions $H + NO_2 \rightarrow HNO_2$ and $H + HNO_2 \rightarrow NO + H_2O$. Thus, the production of water is correlated to the concentration of surface hydrogen atoms. In addition, Koel has reported that NO_2 has a strong interaction with water on Au(111) and can stabilize water resulting in desorption at a higher temperature.[49] Figure S3 indicates that water can be stabilized by NO_2 on the surface yielding a desorption peak temperature at ~190 K. This is in agreement with the TPD spectra for water in Figure 2b: (1) at t = 5 s NO_2 is fully converted to NO via an HNO_2 intermediate and thus is unavailable to interact with the adsorbed water, so there is a single water desorption feature at ~150 K; (2) at t = 10 s NO_2 is produced via N_2O_3 decomposition and interacts with water, shifting the desorption feature to the higher temperature of ~190 K; (3) with further NO_2 impingement, and the surface reaction progressing (to t = 15 and 20 s) more water is generated on the surface and induces a desorption feature again at 160 K. In addition, Figure S4 shows TPD experiments with fixed NO_2 coverage but varying H coverages on Au(111). Figure S4b shows that water has a single desorption feature at ~190 K for low H coverages and induces the other desorption feature at ~160 K with increasing H coverages (i.e., more water is formed). This series of experiments clearly indicates that water desorption is NO_2 concentration dependent on coadsorbed H/Au(111), consistent with the above discussion.

3.4. Infrared Studies to Investigate Reaction Intermediates.

To enhance microscopic understanding of NO_2 reduction, vibrational spectroscopy was employed to study the Au(111) surface coadsorbed with H adatoms and NO_2 at 77 K. Figure 4a shows vibrational spectra for NO_2 on clean Au(111) with varying coverages as a control experiment, and the infrared spectra are in excellent agreement with previously published results by Wang and Koel.[49,50] The distinct absorption peaks for fundamental vibrational modes of NO_2 are evident at 1182 and 808 cm^{-1} which correspond to $\nu(NO_2)$ (symmetric and asymmetric stretching vibrations) and $\delta_s(NO_2)$ (symmetric bending mode) normal modes, respectively. At θ = 1.0 ML, the dimer of NO_2 is formed with the features for N_2O_4 at 1759, 1298, and 784 cm^{-1} which are attributed to the $\nu_a(NO_2)$, $\nu_s(NO_2)$, and $\delta_s(NO_2)$ modes, respectively. In addition, peaks are apparent at 1907 and 1256 cm^{-1} indicating features for N_2O_3 with the $\nu(NO)$ and $\nu_a(NO_2)$ modes, which are reported by Wang and Koel from the reaction between background NO and surface NO_2.[50]

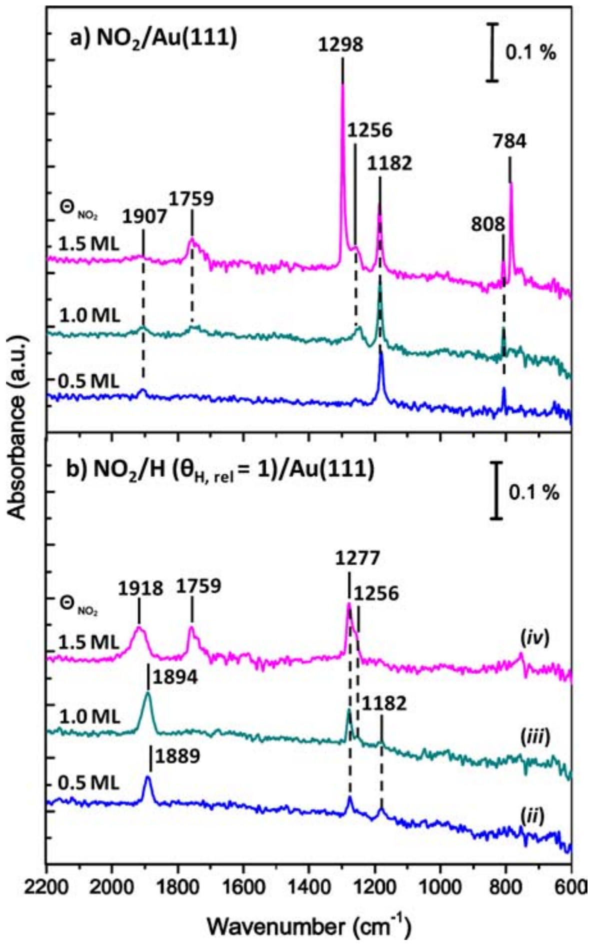

Figure 4. RAIRS spectra of NO_2. RAIRS measurements were conducted on (a) clean Au(111) and (b) $\theta_{H,rel}$ = 1 of H precovered Au(111). In MRBS experiments, NO_2 was impinged onto H/Au(111) at 77 K reaching the end of the induction period (the beginning of NO evolution) at point (ii), the peak of NO evolution at point (iii), and the end of NO evolution at point (iv) as illustrated in Figure 1b. Note that (a) and (b) have the same scale for the Y-axis.

After adsorbing NO_2 on the H precovered surface and achieving a variety of reaction stages [(ii−iv)], we acquired RAIRS spectra at 77 K revealing significant differences in comparison to the control experiments on the clean surface. Figure 4b shows most of the characteristic features for NO_2, N_2O_4, and N_2O_3 on H/Au(111), however the intensities are noticeably diminished compared to Figure 4a, indicating a decrease in the NO_2 concentration due to the reaction with H adatoms. However, with H coadsorbed on the surface, we observe a new feature located in the range of 1850−2000 cm^{-1}, which could result from reaction intermediates, HNO_2 and N_2O_3. We propose this band be assigned to the $\nu(NO)$ mode in HNO_2 or in N_2O_3, respectively. The transformation from HNO_2 to N_2O_3 with NO_2 coverage increasing on the surface blue-shifts the new feature from 1889 to 1918 cm^{-1}. Additionally, we examined the IR spectra after heating the surface to various temperatures regarding those three stages as shown in Figure S5. The feature at 1889 cm^{-1} decreases upon heating the surface to 125 K. In contrast, the 1918 cm^{-1} feature is more stable and remains constant until annealing the sample to 150 K. This observation confirms that those two features are responsible for the different surface species, HNO_2 and N_2O_3. We also note that a feature at 1182 cm^{-1} appears when heating the surface to above 150 K, indicating the formation of NO_2 which likely stems from the decomposition of N_2O_3. The surface infrared spectroscopy measurements at various reaction stages show consistency with MBRS, TPD, and DFT results, clarifying the formation of two intermediates (HNO_2 and N_2O_3).

4. CONCLUSIONS

In summary, we have observed NO_2 reduction to NO on the H atom precovered Au(111) surface at 77 K. During MBRS measurements, adsorbing NO_2 on H/Au(111) causes NO to evolve from the surface at 77 K after a brief induction period. The reaction during the induction period yields a high NO_2 conversion (100%) and remarkable selectivity (100%) toward NO (for low NO_2 coverages with annealing to 120 K) revealing unique catalytic properties for gold in hydrogenation reactions. TPD investigations also provide detailed information demonstrating the production of NO and water upon heating the surface. A mechanism is proposed concerning HNO_2 and N_2O_3 as intermediates which are identified by infrared spectroscopy and DFT calculations. Further, this study shows that weakly bound hydrogen plays a key role in hydrogenation chemistry on gold surfaces and provides some fundamental understanding of the high activity of gold-based catalysts for selective hydrogenation processes.

■ ASSOCIATED CONTENT

Ⓢ Supporting Information

Original data for NO_2 reduction at 77 K; MBRS experimental results for NO_2 reduction with varying H (and D) coverages and subsequent TPD measurements; interaction of water with NO_2 on Au(111); IR spectra acquired from Au(111) with coadsorption of NO_2 and H upon annealing the sample to various temperatures. This material is available free of charge via the Internet at http://pubs.acs.org.

■ AUTHOR INFORMATION

Corresponding Author

mullins@che.utexas.edu

Present Address

[§]Fuel Cell Research Center, Korea Institute of Science and Technology (KIST), Seoul, 136−791, Republic of Korea

Notes

The authors declare no competing financial interest.

■ ACKNOWLEDGMENTS

We acknowledge the generous support of the Department of Energy (DE-FG02-04ER15587) and the Welch Foundation (F-1436 for C.B.M. and F-1535 for G.S.H.). Ming Pan acknowledges the William S. Livingston Fellowship for financial support.

■ REFERENCES

(1) Haruta, M.; Kobayashi, T.; Sano, H.; Yamada, N. *Chem. Lett.* **1987**, 405−408.

(2) Gong, J. L.; Mullins, C. B. *J. Am. Chem. Soc.* **2008**, *130*, 16458−16459.

(3) Cumaranatunge, L.; Delgass, W. N. *J. Catal.* **2005**, *232*, 38−42.

(4) Kim, T. S.; Stiehl, J. D.; Reeves, C. T.; Meyer, R. J.; Mullins, C. B. *J. Am. Chem. Soc.* **2003**, *125*, 2018−2019.

(5) Fu, Q.; Saltsburg, H.; Flytzani-Stephanopoulos, M. *Science* **2003**, *301*, 935−938.

(6) Gong, J. L.; Mullins, C. B. *Acc. Chem. Res.* **2009**, *42*, 1063−1073.

(7) Min, B. K.; Friend, C. M. *Chem. Rev.* **2007**, *107*, 2709−2724.

(8) Xu, B.; Liu, X.; Haubrich, J.; Friend, C. M. *Nature Chem.* **2010**, *2*, 61−65.

(9) Epling, W. S.; Hoflund, G. B.; Weaver, J. F.; Tsubota, S.; Haruta, M. *J. Phys. Chem.* **1996**, *100*, 9929−9934.

(10) Kim, J.; Dohnalek, Z.; Kay, B. D. *J. Am. Chem. Soc.* **2005**, *127*, 14592−14593.

(11) Schumacher, N.; Boisen, A.; Dahl, S.; Gokhale, A. A.; Kandoi, S.; Grabow, L. C.; Dumesic, J. A.; Mavrikakis, M.; Chorkendorff, I. *J. Catal.* **2005**, *229*, 265−275.

(12) Rodriguez, J. A.; Ma, S.; Liu, P.; Hrbek, J.; Evans, J.; Perez, M. *Science* **2007**, *318*, 1757−1760.

(13) Sakurai, H.; Tsubota, S.; Haruta, M. *Appl. Catal., A* **1993**, *102*, 125−136.

(14) Hugon, A.; Delannoy, L.; Louis, C. *Gold Bull.* **2008**, *41*, 127−138.

(15) Galvagno, S.; Schwank, J.; Parravano, G. *J. Catal.* **1980**, *61*, 223−231.

(16) Cardenas-Lizana, F.; Gomez-Quero, S.; Idriss, H.; Keane, M. A. *J. Catal.* **2009**, *268*, 223−234.

(17) Gluhoi, A. C.; Bakker, J. W.; Nieuwenhuys, B. E. *Catal. Today* **2011**, *154*, 13−20.

(18) Mohr, C.; Hofmeister, H.; Radnik, J.; Claus, P. *J. Am. Chem. Soc.* **2003**, *125*, 1905−1911.

(19) Choudhary, T. V.; Sivadinarayana, C.; Datye, A. K.; Kumar, D.; Goodman, D. W. *Catal. Lett.* **2003**, *86*, 1−8.

(20) Jia, J. F.; Haraki, K.; Kondo, J. N.; Domen, K.; Tamaru, K. *J. Phys. Chem. B* **2000**, *104*, 11153−11156.

(21) Corma, A.; Serna, P. *Science* **2006**, *313*, 332−334.

(22) Galvagno, S.; Parravano, G. *J. Catal.* **1978**, *55*, 178−190.

(23) Salama, T. M.; Ohnishi, R.; Shido, T.; Ichikawa, M. *J. Catal.* **1996**, *162*, 169−178.

(24) Nguyen, L. Q.; Salim, C.; Hinode, H. *Appl. Catal., B* **2010**, *96*, 299−306.

(25) Ilieva, L.; Pantaleo, G.; Sobczak, J. W.; Ivanov, I.; Venezia, A. M.; Andreeva, D. *Appl. Catal., B* **2007**, *76*, 107−114.

(26) Kantcheva, M.; Samarskaya, O.; Ilieva, L.; Pantaleo, G.; Venezia, A. M.; Andreeva, D. *Appl. Catal., B* **2009**, *88*, 113−126.

(27) Pan, M.; Pozun, Z. D.; Yu, W.-Y.; Henkelman, G.; Mullins, C. B. *J. Phys. Chem. Lett.* **2012**, *3*, 1894−1899.

(28) Pan, M.; Pozun, Z. D.; Brush, A. J.; Henkelman, G.; Mullins, C. B. *ChemCatChem* **2012**, *4*, 1241−1244.

(29) Sault, A. G.; Madix, R. J.; Campbell, C. T. *Surf. Sci.* **1986**, *169*, 347−356.

(30) Hammer, B.; Norskov, J. K. *Nature* **1995**, *376*, 238−240.

(31) Fujitani, T.; Nakamura, I.; Akita, T.; Okumura, M.; Haruta, M. *Angew. Chem., Int. Ed.* **2009**, *48*, 9515−9518.

(32) Davis, J. E.; Karseboom, S. G.; Nolan, P. D.; Mullins, C. B. *J. Chem. Phys.* **1996**, *105*, 8362−8375.

(33) Davis, J. E.; Nolan, P. D.; Karseboom, S. G.; Mullins, C. B. *J. Chem. Phys.* **1997**, *107*, 943−952.

(34) Pan, M.; Hoang, S.; Gong, J.; Mullins, C. B. *Chem. Commun.* **2009**, 7300−7302.

(35) Pan, M.; Hoang, S.; Mullins, C. B. *Catal. Today* **2011**, *160*, 198−203.

(36) Bartram, M. E.; Koel, B. E. *Surf. Sci.* **1989**, *213*, 137−156.

(37) Saliba, N.; Parker, D. H.; Koel, B. E. *Surf. Sci.* **1998**, *410*, 270−282.

(38) Flaherty, D. W.; Berglund, S. P.; Mullins, C. B. *J. Catal.* **2010**, *269*, 33−43.

(39) Bischler, U.; Bertel, E. *J. Vac. Sci. Technol., A* **1993**, *11*, 458−460.

(40) Bornscheuer, K. H.; Lucas, S. R.; Choyke, W. J.; Partlow, W. D.; Yates, J. T. *J. Vac. Sci. Technol., A* **1993**, *11*, 2822−2826.

(41) Hoang, S.; Pan, M.; Mullins, C. B. *J. Phys. Chem. C* **2009**, *113*, 21745−21754.

(42) Perdew, J. P.; Wang, Y. *Phys. Rev. B* **1992**, *45*, 13244−13249.

(43) Kresse, G.; Furthmuller, J. *VASP the guide*; Vienna University of Technology: Vienna, Austria, 2001.

(44) Blochl, P. E. *Phys. Rev. B* **1994**, *50*, 17953−17979.

(45) Henkelman, G.; Uberuaga, B. P.; Jonsson, H. *J. Chem. Phys.* **2000**, *113*, 9901−9904.

(46) McClure, S. M.; Kim, T. S.; Stiehl, J. D.; Tanaka, P. L.; Mullins, C. B. *J. Phys. Chem. B* **2004**, *108*, 17952−17958.

(47) Ojifinni, R. A.; Froemming, N. S.; Gong, J.; Pan, M.; Kim, T. S.; White, J. M.; Henkelman, G.; Mullins, C. B. *J. Am. Chem. Soc.* **2008**, *130*, 6801−6812.

(48) Pan, M.; Flaherty, D. W.; Mullins, C. B. *J. Phys. Chem. Lett.* **2011**, 1363−1367.

(49) Wang, J.; Koel, B. E. *Surf. Sci.* **1999**, *436*, 15−28.

(50) Wang, J.; Koel, B. E. *J. Phys. Chem. A* **1998**, *102*, 8573−8579.